

Iron Catalysis

Mechanistic Studies on NaHCO₃ Hydrogenation and HCOOH Dehydrogenation Reactions Catalysed by a Fe^{II} Linear Tetrphosphine ComplexRocío Marcos,^[a] Federica Bertini,^[b] Zilvinas Rinkevicius,^[a] Maurizio Peruzzini,^[b] Luca Gonsalvi,^[b] and Mårten S. G. Ahlquist*^[a]

Abstract: We present a theoretical extension of the previously published bicarbonate hydrogenation to formate and formic acid dehydrogenation catalysed by Fe^{II} complexes bearing the linear tetrphosphine ligand tetraphos-1. The hydrogenation reaction was found to proceed at the singlet surface with two competing pathways: A) H₂ association to the Fe–H species followed by deprotonation to give a Fe(H)₂

intermediate, which then reacts with CO₂ to give formate. B) CO₂ insertion into the Fe–H bond, followed by H₂ association and subsequent deprotonation. B was found to be slightly preferred with an activation energy of 22.8 kcal mol⁻¹, compared to 25.3 for A. Further we have reassigned the Fe–H complex, as a Fe(H)(H₂), which undergoes extremely rapid hydrogen exchange.

Introduction

The hydrogenation of CO₂ or NaHCO₃ to HCOOH or NaHCO₂ are important reactions, which hold promise within carbon dioxide utilisation processes to obtain higher added-value chemicals. If combined with its reverse reaction, HCOOH dehydrogenation (FADH), a carbon-neutral hydrogen storage and release cycle can be envisaged, as recently demonstrated by various research groups worldwide.^[1] In order to bring about bicarbonate hydrogenation (BCH) with high yields, the reaction needs the presence of a catalyst. Many solutions have been proposed, generally based on noble transition metals, which have intrinsically the drawback of being rare and expensive.^[2] Iron is a particularly attractive metal in catalysis as it is abundant, environmentally benign and generally non-toxic, and inexpensive compared to noble metal-based catalysts.^[3] Iron catalysts containing various types of P-based ligands have been reported in the last few years for these reactions, and in particular multidentate phosphines^[4,5] and pincer-type ligands^[6] gave the best performance for CO₂ and/or NaHCO₃ reduction. To date, the highest turnover number (TON) described without the use of additives for an iron-based catalyst was obtained

using tetradentate phosphines as ligands. Complexes [FeH(PP₃)]⁺ (PP₃ = P(CH₂CH₂PPh₂)₃) and [FeF(PPhP₃)]⁺ (PPhP₃ = P(C₆H₄PPh₂)₃) described by Beller and co-workers showed remarkable activities for both FADH^[7] and BCH^[4] reactions. Some of us recently reported DFT mechanistic investigations on BCH-FADH reactions in the presence of Beller's catalysts, showing that the solvents used in these reactions play a central role,^[8] that is, changing the solvent the reaction can be reversed. Moreover, it was predicted that for BCH the experimentally used solvent (MeOH) could be replaced with *t*BuOH or DMSO to enhance the activity of the system.

Another active catalytic system for BCH and FADH reactions, obtained in situ from Fe(BF₄)₂ and a linear tetradentate phosphine (tetraphos-1, P₄) as stabilising ligand, has been reported by Gonsalvi and co-workers.^[5] In particular, it was shown that the *rac*-isomer of the ligand gave the best results and in contrast, worse catalytic activities were observed in the presence of the *meso*-P₄ isomer, as the former gave preferentially a *cis-α* conformation in the corresponding Fe^{II} complexes, most suitable for substrate coordination and hydride transfer. By NMR and HP NMR experiments, mechanistic details of both reactions were obtained, and the common active species for both BCH and FADH reactions was proposed to be the monohydrido cationic complex [FeH(*rac*-P₄)]⁺ (**1**) in analogy with Beller's [FeH(PP₃)]⁺ complex. In this paper we report a density functional theory (DFT) calculations study on the mechanism for BCH and FADH reactions in the presence of **1**. By combination of theoretical and new experimental data it was possible to propose reaction pathways for BCH and FADH reactions. The reasons underlying the missing experimental observation of the expected Fe-hydrido dihydrogen intermediate (**2**), derived from H₂ coordination to **1**, are also explained (Figure 1).

[a] Dr. R. Marcos, Prof. Z. Rinkevicius, Prof. M. S. G. Ahlquist
Division of Theoretical Chemistry & Biology, School of Biotechnology
KTH Royal Institute of Technology
109 61 Stockholm (Sweden)
E-mail: ahlqui@kth.se

[b] Dr. F. Bertini, Dr. M. Peruzzini, Dr. L. Gonsalvi
Consiglio Nazionale delle Ricerche (CNR)
Istituto di Chimica dei Composti Organometallici (ICCOM)
Via Madonna del Piano 10, 50019 Sesto Fiorentino, Firenze (Italy)

Supporting information and the ORCID identification number(s) for the author(s) of this article can be found under
<https://doi.org/10.1002/chem.201704927>.

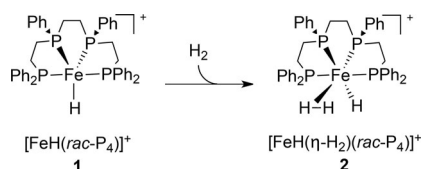


Figure 1. Monohydrido cationic complex $[\text{FeH}(\text{rac-P}_4)]^+$ (**1**) and iron-hydrido dihydrogen intermediate $[\text{FeH}(\eta^2\text{-H}_2)(\text{rac-P}_4)]^+$ (**2**).

Results and Discussion

The first issue for the DFT calculation study was to choose a reliable functional. Based on the reported experimental data^[5] and our previous work on the theoretical investigation^[8] of FADH and BCH reactions on the system described by Beller, Laurency and co-workers,^[4] complex **1** was selected as the initial species for this investigation. In a previous study,^[9] it was shown that $[\text{FeH}(\text{PP}_3)]^+$ has a triplet ground state ($m=3$), which agrees well with our calculated results (Table 1). In con-

Table 1. Calculated free energies ΔG (kcal mol^{-1}) for the singlet and triplet states of $[\text{FeH}(\text{PP}_3)]^+$ and $[\text{FeH}(\text{rac-P}_4)]^+$ (1). ^[a]				
	$[\text{FeH}(\text{PP}_3)]^+$ $m=1$	$[\text{FeH}(\text{PP}_3)]^+$ $m=3$	$[\text{FeH}(\text{rac-P}_4)]^+$ (1) $m=1$	$[\text{FeH}(\text{rac-P}_4)]^+$ (1) $m=3$
B3PW91/M06	17.3	0.0	13.5	0.0
B3PW91/M06-L	6.6	0.0	0.0	0.7
B3PW91/M06-L ^[b]	4.8	0.0	0.0	2.5
[a] Functional/LACV3P**+++. [b] 6-311++G-3df-3pd on phosphorus.				

trast to the PP_3 -based catalyst, complex **1** was experimentally isolated and characterised by NMR in the singlet ground state ($m=1$). However, when we used the same functional of our previous studies, namely B3PW91/M06, complex **1** was found to be more stable in the triplet state than in the singlet state by $13.5 \text{ kcal mol}^{-1}$. In order to understand the reason for this disagreement between the calculated and experimental results, different functionals were tested, since the spin state of metals is highly sensitive to the exchange functional used.

The geometry of **1** was optimised with B3PW91 and LACVP** level core potential and basis set, which was also used for calculating the solvation free energy, the ZPE, the $A_{\text{H}298}$ and the S_{298} terms. The electronic energy was calculated by single point energy corrections with the M06,^[10] M06-L^[11] or M06-L^[4] with a larger 6-311++G-3df-3pd basis set on phosphorus. For iron the LACV3P**++ basis set and core potential was used, which was further augmented with two f-functions at the Fe center with parameters as suggested by Martin and Sundermann.^[12] For all other atoms 6-311++G** was used. The larger basis set on phosphorus was tested in order to evaluate the effect of a more polarised and flexible basis on the spin states. We reasoned that a more flexible basis set could improve the electron back-donation from the metal, which

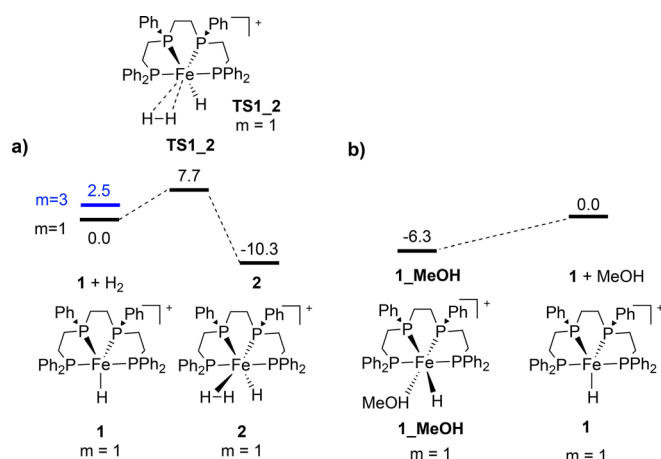
would favour the more tightly bound singlet state. From the results in Table 1 we see that the hybrid functional with a fraction of Hartree–Fock (HF) exchange M06 predicts a triplet ground state for **1**, in disagreement with the experimental results. A better agreement was found with M06-L functional, suggesting that M06-L/LACV3P**++ with 6-311++G-3df-3pd on P method are more reliable for this study. For geometry optimisations and frequency calculations of these species we did not use M06-L since we found it to be less numerically stable for gradients and hessian calculations, and sometimes give artificial imaginary frequencies. We also tested the different functionals for $[\text{FeH}(\text{PP}_3)]^+$ and observed that all agreed with the experimental data and that also for this iron-hydride complex a triplet ground state is more stable than the singlet state even using the M06-L functional (Table 1).

To further test our methodology we performed NEVPT2 calculations on a model system, where all phenyl groups of **1** were replaced by methyl groups. This change would likely affect the singlet triplet splitting, however we could benchmark our methods and we reasoned that the method that agrees for the model complex will also be the better choice for the full system. The computations are described in more detail in the computational details, and both M06-L and NEVPT2 show a clear preference for the singlet configuration over the triplet.

Mechanism of BCH reaction

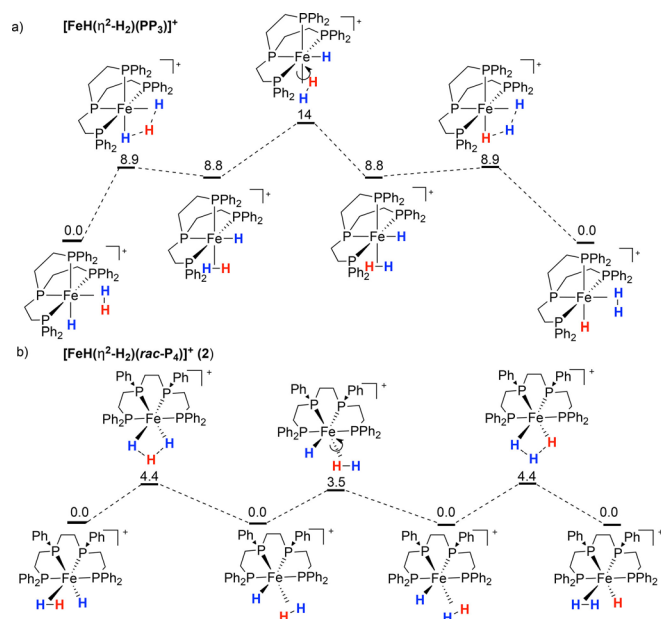
A first striking difference between the Fe-PP_3 and $\text{Fe}(\text{rac-P}_4)$ systems was their observed reactivities with H_2 . Previous studies^[13] showed that the reaction of $[\text{FeH}(\text{PP}_3)]^+$ with H_2 gave the dihydrogen adduct $[\text{FeH}(\eta^2\text{-H}_2)(\text{PP}_3)]^+$. The rate of the exchange of the hydrogen atoms between $\eta^2\text{-H}_2$ and the hydride ligands was determined by low temperature NMR, showing peaks decoalescence at -60°C . The activation free energy for the process was determined as around $12\text{--}13 \text{ kcal mol}^{-1}$. In the case of complex **1**, reaction with H_2 did not show the formation of the expected complex $[\text{FeH}(\eta^2\text{-H}_2)(\text{rac-P}_4)]^+$ (**2**) and only the signal corresponding to the hydrido ligand was observed in the ^1H NMR spectrum even under a pressure of hydrogen at low temperature.^[5] This behaviour was previously described for the corresponding *meso*-isomer complex $[\text{FeH}(\text{meso-P}_4)]^+$.^[14] Thus, we decided to reinvestigate this apparently odd behaviour from a theoretical viewpoint. Indeed, our calculations showed that **2** should be significantly more stable than **1**, with a calculated free energy difference of $-10.3 \text{ kcal mol}^{-1}$ in favour of **2** (Scheme 1a). The H_2 (H1-H2) molecule is tightly bound with a Fe-H1 distance of 1.59 \AA and a Fe-H2 distance of 1.57 \AA . The H1-H2 distance is elongated to 0.87 \AA from 0.74 \AA in vacuum. Moreover, the calculated structures showed that in MeOH a solvent molecule binds strongly to **1** to give the adduct **1_MeOH**, with an energy gain of $6.3 \text{ kcal mol}^{-1}$ (Scheme 1b), in turn suggesting that the putative pentacoordinate geometry assumed for **1** should be disfavoured in presence of coordinating molecules such as H_2 or MeOH.

A possible explanation for the lack of decoalescence of the NMR signals of **2** could be that the rate of hydrogen exchange



Scheme 1. Free energy profiles calculated starting with **1**. The relative solvation corrected Gibbs free energies (in MeOH) are given in kcal mol⁻¹.

is too fast at the NMR timescale to be observed even at low temperature. We therefore calculated the exchange mechanism for $[\text{FeH}(\eta^2\text{-H}_2)(\text{PP}_3)]^+$ and **2** (Scheme 2). The former complex has two inequivalent sites and the mechanism for exchange of the hydrogens atoms of the H_2 and the hydride involves initial formation of the higher energy isomer, followed by rotation of the H_2 ligand and finally reformation of hydrido-dihydrogen complex. The highest point on the calculated free energy surface is the rotation of the $\eta^2\text{-H}_2$ ligand at 14 kcal mol⁻¹, in good agreement with the experimental value of 12–13 kcal mol⁻¹.^[13a] In the case of **2** the formation for the hydride dihydrogen isomer is thermoneutral, since the two coordination sites are symmetric. The activation energy is predicted to be much lower than in the previous complex, only 4.4 kcal mol⁻¹. The rotation of the $\eta^2\text{-H}_2$ ligand is also facile with a cal-



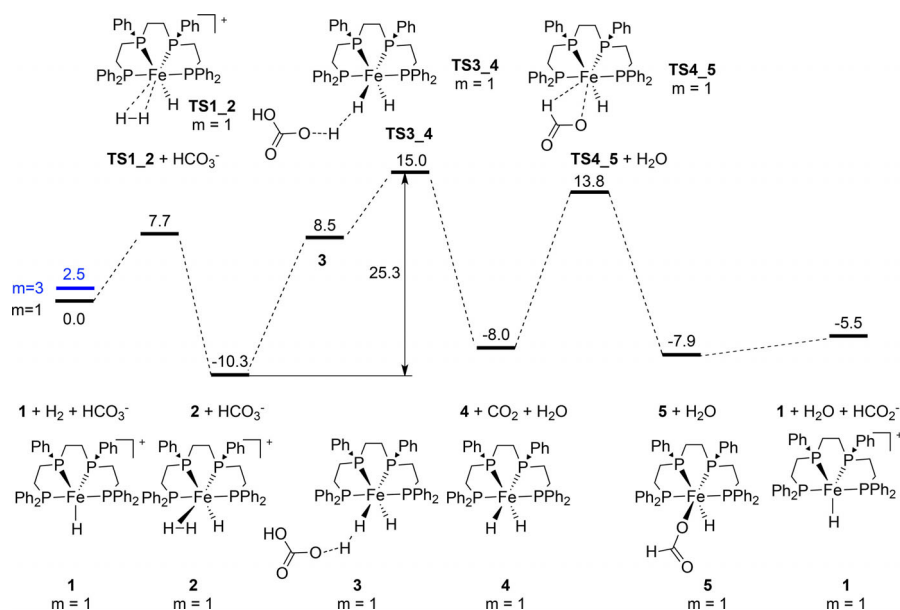
Scheme 2. Free energy profiles for hydrogen-hydride ligand exchange for (a) $[\text{FeH}(\eta^2\text{-H}_2)(\text{PP}_3)]^+$ and (b) $[\text{FeH}(\eta^2\text{-H}_2)(\text{rac-P}_4)]^+$ (**2**). The relative solvation corrected Gibbs free energies (in MeOH) are given in kcal mol⁻¹.

culated activation energy of merely 3.5 kcal mol⁻¹. This result indicates that even at low temperature decoalescence should not be observed and that under a pressure of hydrogen, complex **1** most likely should give **2**.

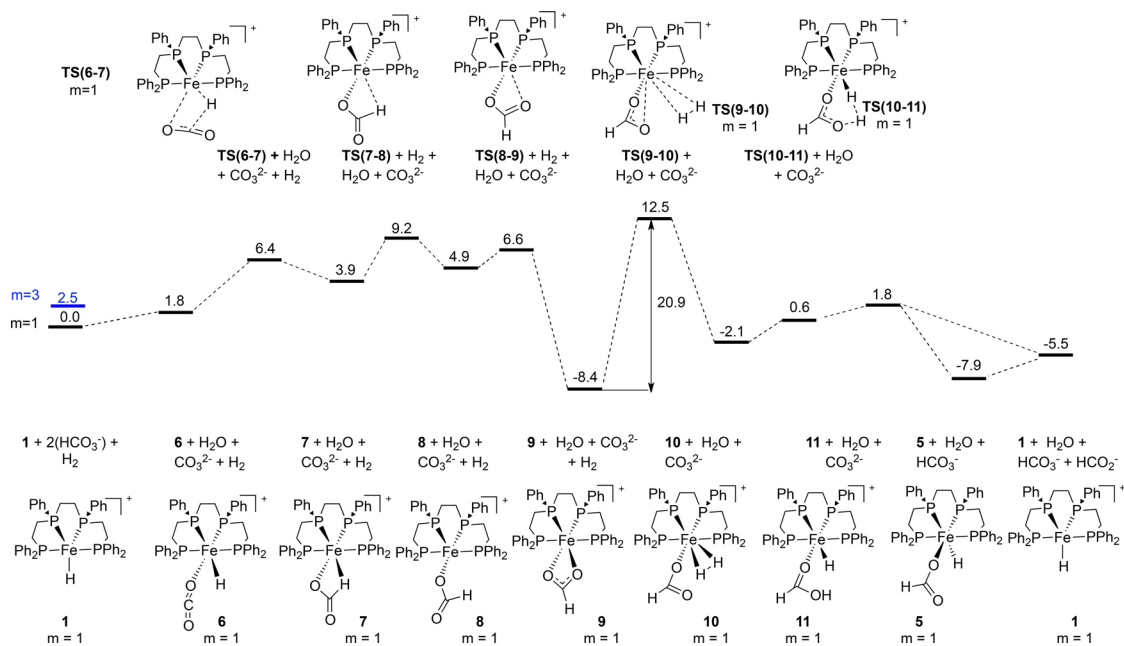
We then tried to further support the computational results and prove indirectly the formation of **2** by experimental methods. *Rac-P*₄ (20 mg; 0.03 mmol), $\text{Fe}(\text{BF}_4)_2 \cdot 6\text{H}_2\text{O}$ (10 mg; 0.03 mmol) and 1 mL $[\text{D}_8]\text{THF}$ were placed into a screw cap NMR tube, resulting in the formation of a deep purple suspension. In the $^{31}\text{P}\{\text{H}\}$ NMR spectrum no signals were observed at this stage due to the low solubility of the purple complex. 0.5 mL of propylene carbonate (PC) were added to dissolve the purple complex, affording a clear deep purple solution. $^{31}\text{P}\{\text{H}\}$ NMR analysis showed two broad signals of equal intensities at 97.0 and 57.9 ppm, which are typically observed upon mixing *rac-P*₄ and $\text{Fe}(\text{BF}_4)_2 \cdot 6\text{H}_2\text{O}$ in PC alone, and other two weaker signals of triplet appearance at 99.9 and 55.4 ppm, which are due to THF coordination to the *(rac-P*₄)Fe moiety, as previously observed by addition of MeOH or CD_3OD , in PC.^[15] H_2 (1 bar) was then bubbled into the purple solution until it turned light pink (ca. 1 min), resulting in the quantitative formation of a new complex characterized by two triplets at 116.9 and 96.3 ppm. These $^{31}\text{P}\{\text{H}\}$ NMR signals correspond to those that were previously attributed to the in situ formed monohydride complex **1**,⁵ albeit slightly shifted due to the use of a different solvent mixture. Accordingly, a broad triplet was observed in the hydride region ($\delta_{\text{H}} = -10.9$ ppm). Next, NEt_3 (80 μL) were added to this mixture, which turned into a bright yellow solution. $^{31}\text{P}\{\text{H}\}$ NMR analysis showed two new peaks at 123.4 and 112.7 ppm, which we attributed to dihydride $[\text{FeH}_2(\text{rac-P}_4)]$ (**4**; reported values for the isolated complex **4** in pure $[\text{D}_8]\text{THF}$: $\delta_{\text{P}} = 123.8$ and 113.1 ppm). The corresponding Fe–hydride signal was observed around -13 ppm in the ^1H NMR spectrum.

The formation of dihydride **4** by treatment of the described mixture obtained from *rac-P*₄, $\text{Fe}(\text{BF}_4)_2 \cdot 6\text{H}_2\text{O}$ and H_2 with a base provides indirect evidence for the formation of **2**, namely by deprotonation of the $\eta^2\text{-H}_2$ ligand.

Next, we set out to calculate the reaction pathway for the Fe-catalysed reduction of bicarbonate (BCH). Two possible mechanisms were investigated, namely Pathway A, where a dihydrogen molecule coordinates first to **1** (Scheme 3) and Pathway B, where CO_2 coordinates first to **1** (Scheme 4). In Pathway A, the first step is the coordination of H_2 to **1** to form **2**. The second step is the deprotonation of the $\eta^2\text{-H}_2$ ligand by a bicarbonate molecule to form the neutral dihydrido complex $[\text{Fe}(\text{H})_2(\text{rac-P}_4)]$ (**4**) and carbonic acid, which proceeds via **TS3 4** with a free energy barrier of 25.3 kcal mol⁻¹ relative to **2**. Prior to the H–H cleavage an ionpair complex **3** is formed, in a step that was found to be endergonic. We could like to note that steps involving formation or combination of charged species are more likely associated with larger errors, simply due to the magnitude of the free energy of solvation, meaning that even small percental errors could be of large magnitude. The carbonic acid that is generated in this step is then assumed to generate water and CO_2 , and CO_2 insertion into the Fe–H bond of **4** yields the hydrido-formate complex



Scheme 3. Free energy profiles for BCH reaction via Pathway A starting from **1**. The relative solvation corrected Gibbs free energies (in MeOH) are given in kcal mol⁻¹.



Scheme 4. Free energy profiles for BCH reaction via Pathway B starting from **1**. The relative solvation corrected Gibbs free energies (in MeOH) are given in kcal mol⁻¹.

[FeH(O₂CH)(*rac*-P₄)] (**5**) via **TS4–5** with a free energy barrier of 21.8 kcal mol⁻¹. The elimination of the formate molecule from **5** regenerates complex **1** and completes the cycle. Thus, the (η^2 -H₂) ligand deprotonation step from **2** is the rate-determining step of the reaction in this pathway.

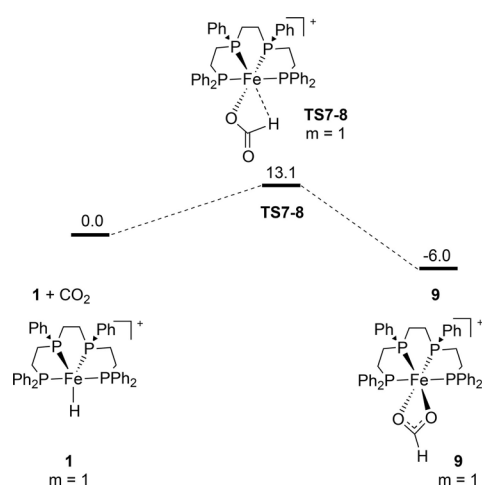
In Pathway B (Scheme 4), the reaction was assumed to be initiated by two HCO₃⁻ disproportionating to CO₂, H₂O and CO₃²⁻. This reaction is slow but observable at room temperature in sea water,^[15] but should be accelerated at the reaction temperature and higher bicarbonate concentrations in the cur-

rent catalytic system. This step is followed by coordination of CO₂ to **1**, then insertion of CO₂ in the Fe–H bond to generate the Fe formate complex [Fe(O₂CH)(*rac*-P₄)]⁺ (**9**). The rate determining step of this mechanism is the coordination of hydrogen to **9**, which first gives complex [Fe(η^2 -H₂)(O₂CH)(*rac*-P₄)]⁺ (**10**). The free energy barrier of this transition state, **TS(9–10)**, is 20.9 kcal mol⁻¹ from **9**. If we consider **2** as the resting state then the free energy barrier is 22.8 kcal mol⁻¹. From **10**, deprotonation of the Fe-coordinated dihydrogen molecule occurs intramolecularly resulting in intermediate **11**, where a FA mole-

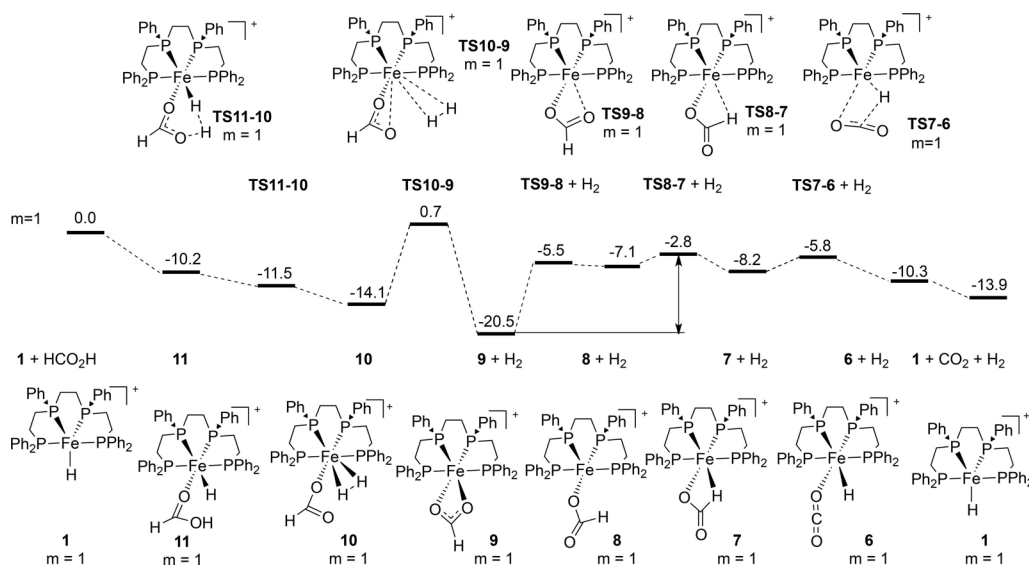
cule is bonded to the regenerated $[\text{Fe}(\text{H})(\text{rac-P}_4)]^+$ fragment. The FA then loses a proton to solution and the formate finally leaves to regenerate **1**.

Mechanism B thus seems to be the preferred pathway starting from **1** for BCH reaction, having a lower energy barrier. In both cases the overall reaction is exergonic with a reaction free energy of $-5.5 \text{ kcal mol}^{-1}$, which is in good agreement with the experimental results.^[5]

One experimental result to control against is the reaction where **1** with CO_2 in THF to give $[\text{Fe}(\eta^2\text{-O}_2\text{CH})(\text{rac-P}_4)]\text{BPh}_4$. Our calculations agree well with the reactivity showed in experimental results (Scheme 5). The formation of the coordinated formate complex **9** is exergonic by $-6.0 \text{ kcal mol}^{-1}$ respect to **1**, which indicates a significant thermodynamic driving force. The activation energy of $13.1 \text{ kcal mol}^{-1}$ indicates also a high rate for the insertion, in agreement with the experiments.



Scheme 5. Free energy profiles for CO_2 insertion starting with **1**. The relative solvation corrected Gibbs free energies (in tetrahydrofuran which was the solvent used in this particular experiment) are given in kcal mol^{-1} .



Scheme 6. Free energy profiles for FADH reaction starting from **1**. The relative solvation corrected Gibbs free energies in kcal mol^{-1} (solvent continuum model used parameters dimethyl sulfoxide as a model for the experimentally used propylene carbonate).

Mechanism of FADH reaction

The reverse reaction of BCH, namely FADH, was also modelled by DFT calculations methods (Scheme 6). Reaction of **1** with HCOOH initially forms the formic acid hydrido complex **11**. Intramolecular protonation of the hydrido ligand by the coordinated acid follows, giving complex $[\text{Fe}(\text{O}_2\text{CH})(\eta^2\text{-H}_2)(\text{rac-P}_4)]^+$ (**10**) in turn. Hydrogen elimination and binding of the formate anion to the Fe metal centre in a $\kappa^2\text{-O,O}$ fashion generates complex **9**. The free energy barrier of this step (TS10-9) is calculated to $14.8 \text{ kcal mol}^{-1}$ relative to **10**. Subsequent decoordination of one of the oxygen atoms of the formate and coordination of the hydrogen generates the $\kappa^2\text{-O,H}$ formate intermediate **7**. This isomerisation step is the rate determining step of the reaction with a free energy barrier of $17.7 \text{ kcal mol}^{-1}$. Then β -hydride elimination from complex **7** yields complex **6** which regenerates the iron hydride complex **1** by CO_2 elimination closing the cycle. The complex **2** lies at $-10.5 \text{ kcal mol}^{-1}$ with respect to **1** so the formate coordinated complex **9** is preferentially formed under these conditions, as observed experimentally. The computed mechanism for the FADH process is in accord with previously reported experimental studies, which highlighted the role of hydride and formate complexes **1** and **9** as key intermediates.

Conclusion

In summary, the mechanism of the Fe-catalysed hydrogenation of bicarbonate in the presence of a Fe^{II} complex stabilised by the tetradentate linear phosphine *rac-P*₄ has been elucidated by DFT methods, and the active species was reassigned based on theoretical and experimental results. Two different pathways were proposed as possible candidates with similar activation free energies. The pathway that appears to be more favourable is the one where two bicarbonate anions were disproportionated to carbonate, water and carbon dioxide which

coordinates to the iron hydride pre-catalyst. The activation energy was calculated at $22.8 \text{ kcal mol}^{-1}$. This activation energy is relative to the most stable structure in presence of H_2 , $[\text{FeH}(\eta^2\text{-H}_2)(\text{rac-P}_4)]^+$. This species was found to be the complex that was previously assigned as the monohydride, experimentally. We showed here that the absence of decoalescence of the hydride peak at low temperature in the $^1\text{H-NMR}$ was due to extremely rapid exchange of the hydrogen atoms in the complex. The alternative reaction mechanism was initiated by reaction between the $[\text{FeH}(\eta^2\text{-H}_2)(\text{rac-P}_4)]^+$ and bicarbonate to generate $[\text{Fe}(\text{H}_2)(\text{rac-P}_4)]$. The dihydride complex could then react with the CO_2 generated from the carbonic acid in the first step to give the $[\text{FeH}(\text{O}_2\text{CH})(\text{rac-P}_4)]$ complex. The activation energy of this mechanism was calculated to be slightly higher at $25.3 \text{ kcal mol}^{-1}$. In addition, the mechanism of formic acid dehydrogenation in the presence of the same pre-catalyst has been calculated and found to be in agreement with the experimental results

Computational Details

All geometry optimisations were performed with Jaguar 7.6,^[16] using B3PW91^[17] and the LACVP** basis set and core potential.^[18] Harmonic frequency analyses were performed on each geometry to confirm that it had no negative vibrational frequencies for ground states, and one single imaginary vibrational frequency for transition states. Single point solvation free energies of all Fe complexes were calculated using the PBF solvation model in Jaguar.^[19] For all small molecules and ions SM8 was used since it generally gives more accurate values.^[20] The doubly anionic carbonate was solvated by two explicit methanol molecules. To describe propylene carbonate we used parameters for DMSO since the two has similar size and dielectric constant, and both are aprotic solvents. For the final electronic energies, we used the M06-L functional in combination with the LACV3P**++ basis set and core potential^[21] for iron which employs the 6-311++G** for all other atoms. The iron basis was further extended with two f-functions with exponents set to the values suggested by Martin.^[12] For phosphorous we used the larger 6-311++G-3df-3pd basis for adequate treatment of the polarisation of the phosphorus due to the coordination to the metal. Our choice of the M06-L functional was based on its general good performance for both main group elements, transition metals, activation energies, and its reasonable ability to predict the correct spin state of a model complex.^[22] This benchmark was performed with ORCA 4.0 using NEVPT2^[23] calculations of singlet and triplet states of iron complex **1-Me**, which is **1** with all phenyl groups replaced by methyl groups. The calculations were carried out using common CAS space of 10 electrons in 10 orbitals. The molecular orbitals included in CAS space have been selected from analysis of natural orbitals obtained with CEPA-2 method.^[24] All calculations we have been carried out in def2-TZVP basis set.^[25] The singlet/triplet splitting was calculated to $9.9 \text{ kcal mol}^{-1}$ in favor of the singlet. M06-L/ LACV3P**++(6-311++G-3df-3pd) gave $4.8 \text{ kcal mol}^{-1}$, which is a bit lower compared to the NEVPT2 calculations, but still in favor of the singlet. Gibbs free energies were finally calculated for each species $G_{\text{M06}} = E_{(\text{M06/LACV3P}^{**++} + 2f \text{ on Fe})} + G_{\text{solv}} + \text{ZPE} + \text{H}_{298} - \text{TS}_{298}$. A concentration correction of $1.9 \text{ kcal mol}^{-1}$ was added for solvated species, as Jaguar by default uses 1 M gas concentration instead of 1 atm.

Experimental Section

Experimental procedures and NMR spectra are included in the Supporting Information.

Acknowledgements

Computational resources have been provided by the National Supercomputer Centre in Linköping, Sweden. Financial support has been received from Vetenskapsrådet. This work was also supported by COST Action 1025 CARISMA (Catalytic Routines for Small Molecule Activation). L.G. thanks ECRF for financial support by ENERGILAB Project.

Conflict of interest

The authors declare no conflict of interest.

Keywords: catalysis · CO_2 hydrogenation · density functional theory · iron · reaction mechanisms

- [1] a) A. K. Singh, S. Singh, A. Kumar, *Catal. Sci. Technol.* **2016**, *6*, 12–40; b) D. Mellmann, P. Sponholz, H. Junge, M. Beller, *Chem. Soc. Rev.* **2016**, *45*, 3954–3988; c) F. Joó, *ChemSusChem* **2008**, *1*, 805–808; d) S. Enthaler, J. von Langermann, T. Schmidt, *Energy Environ. Sci.* **2010**, *3*, 1207–1217; e) B. Loges, A. Boddien, F. Gärtner, H. Junge, M. Beller, *Top. Catal.* **2010**, *53*, 902–914; f) J. Klankermayer, S. Wesselbaum, K. Beydoun, W. Leitner, *Angew. Chem. Int. Ed.* **2016**, *55*, 7296–7343; *Angew. Chem.* **2016**, *128*, 7416–7467 (and references therein).
- [2] a) Y. Himeda, *Green Chem.* **2009**, *11*, 2018–2022; b) Y. Himeda, N. Onozawa-Komatsuzaki, H. Sugihara, K. Kasuga, *Organometallics* **2007**, *26*, 702–712; c) Y. Himeda, N. Onozawa-Komatsuzaki, H. Sugihara, K. Kasuga, *J. Photochem. Photobiol. A* **2006**, *182*, 306–309; d) Y. Himeda, N. Onozawa-Komatsuzaki, H. Sugihara, H. Arakawa, K. Kasuga, *Organometallics* **2004**, *23*, 1480–1483; e) G. Papp, J. Csorba, G. Laurency, F. Joó, *Angew. Chem. Int. Ed.* **2011**, *50*, 10433–10435; *Angew. Chem.* **2011**, *123*, 10617–10619; f) J. A. Elek, L. Nádasdi, G. Papp, G. Laurency, F. Joó, *Appl. Catal. A* **2003**, *255*, 59–67; g) A. Kathó, Z. Opre, G. Laurency, F. Joó, *J. Mol. Catal. A* **2003**, *204*–205, 143–148; h) F. Joó, G. Laurency, P. Karády, L. Nádasdi, R. Roulet, *Appl. Organomet. Chem.* **2000**, *14*, 857–859; i) G. Laurency, F. Joó, L. Nádasdi, *High Press. Res.* **2000**, *18*, 251–255; j) G. Laurency, F. Joó, L. Nádasdi, *Inorg. Chem.* **2000**, *39*, 5083–5088; k) F. Joó, G. Laurency, L. Nádasdi, J. Elek, *Chem. Commun.* **1999**, 971–972; l) C. Federsel, R. Jackstell, A. Boddien, G. Laurency, M. Beller, *ChemSusChem* **2010**, *3*, 1048–1050; m) A. Boddien, F. Gärtner, C. Federsel, P. Sponholz, D. Mellmann, R. Jackstell, H. Junge, M. Beller, *Angew. Chem. Int. Ed.* **2011**, *50*, 6411–6414; *Angew. Chem.* **2011**, *123*, 6535–6538; n) J. Elek, L. Nádasdi, G. Papp, G. Laurency, F. Joó, *Appl. Catal. A* **2003**, *255*, 59–67; o) I. Osadchuk, T. Tamm, M. S. G. Ahlquist, *ACS Catal.* **2016**, *6*, 3834–3839; p) I. Osadchuk, T. Tamm, M. S. G. Ahlquist, *Organometallics* **2015**, *34*, 4932–4940; q) M. S. G. Ahlquist, *J. Mol. Catal. A* **2010**, *324*, 3–8.
- [3] For recent reviews see: a) C. Bolm, J. Legros, J. L. Paith, L. Zani, *Chem. Rev.* **2004**, *104*, 6217–6254; b) S. Enthaler, K. Junge, M. Beller, *Angew. Chem. Int. Ed.* **2008**, *47*, 3317–3321; *Angew. Chem.* **2008**, *120*, 3363–3367; c) S. Gaillard, J.-L. Renaud, *ChemSusChem* **2008**, *1*, 505–509; d) R. H. Morris, *Chem. Soc. Rev.* **2009**, *38*, 2282–2291; e) K. Junge, K. Schröder, M. Beller, *Chem. Commun.* **2011**, *47*, 4849–4859; f) M. Carwish, M. Wills, *Catal. Sci. Technol.* **2012**, *2*, 243–255; g) W. H. Bernskoetter, N. Hazari, *Acc. Chem. Res.* **2017**, *50*, 1049–1058.
- [4] For iron complexes with multidentate phosphine ligands see: a) C. Ziebart, C. Federsel, P. Anbarasan, R. Jackstell, W. Baumann, A. Spannenberg, M. Beller, *J. Am. Chem. Soc.* **2012**, *134*, 20701–20704; b) C. Federsel, A. Boddien, R. Jackstell, R. Jennerjahn, P. J. Dyson, R. Scopelliti, G.

- Laurencyzy, M. Beller, *Angew. Chem. Int. Ed.* **2010**, *49*, 9777–9780; *Angew. Chem.* **2010**, *122*, 9971–9974.
- [5] F. Bertini, I. Mellone, A. Ienco, M. Peruzzini, L. Gonsalvi, *ACS Catal.* **2015**, *5*, 1254–1265.
- [6] For iron PNP pincer complexes see: a) F. Bertini, N. Gorgas, B. Stöger, M. Peruzzini, L. F. Veiros, K. Kirchner, L. Gonsalvi, *ACS Catal.* **2016**, *6*, 2889–2893; b) Y. Zhang, A. D. MacIntosh, J. L. Wong, E. A. Bielinski, P. G. Williard, B. Q. Mercado, N. Hazari, W. Bernskoetter, *Chem. Sci.* **2015**, *6*, 4291–4299; c) R. Langer, Y. Diskin-Posner, G. Leitun, L. J. W. ##, Y. Ben-David, D. Milstein, *Angew. Chem. Int. Ed.* **2011**, *50*, 9948–9952; *Angew. Chem.* **2011**, *123*, 10122–10126; d) I. Mellone, N. Gorgas, F. Bertini, M. Peruzzini, K. Kirchner, L. Gonsalvi, *Organometallics* **2016**, *35*, 3344–3349; e) E. A. Bielinski, P. O. Lagaditis, Y. Zhang, B. Q. Mercado, C. Würtele, W. H. Bernskoetter, N. Hazari, S. Schneider, *J. Am. Chem. Soc.* **2014**, *136*, 10234–10237.
- [7] A. Boddien, D. Mellmann, F. Gärtner, R. Jackstell, H. Junge, P. J. Dyson, G. Laurencyzy, R. Ludwig, M. Beller, *Science* **2011**, *333*, 1733–1736.
- [8] a) R. Marcos, L. Xue, R. Sánchez-de-Armas, M. S. G. Ahlquist, *ACS Catal.* **2016**, *6*, 2923–2929; b) R. Sánchez-de-Armas, *Chem. Eur. J.* **2013**, *19*, 11869–11873.
- [9] C. Bianchini, F. Laschi, M. Peruzzini, F. M. Ottaviani, A. Vacca, P. Zanello, *Inorg. Chem.* **1990**, *29*, 3394–3402.
- [10] Y. Zhao, D. G. Truhlar, *Theor. Chem. Acc.* **2008**, *120*, 215–241.
- [11] Y. Zhao, D. G. Truhlar, *J. Chem. Phys.* **2006**, *125*, 194101–194118.
- [12] J. M. L. Martin, A. Sundermann, *J. Chem. Phys.* **2001**, *114*, 3408–3420.
- [13] a) C. Bianchini, M. Peruzzini, F. Zanobini, *J. Organomet. Chem.* **1988**, *354*, C19–C22; b) C. Bianchini, D. Masi, M. Peruzzini, *Inorg. Chem.* **1997**, *36*, 1061–1069.
- [14] a) M. T. Bautista, K. A. Earl, P. A. Maltby, R. H. Morris, *J. Am. Chem. Soc.* **1988**, *110*, 4056–4057; b) M. T. Bautista, K. A. Earl, P. A. Maltby, R. H. Morris, C. T. Schweitzer, *Can. J. Chem.* **1994**, *72*, 547–560.
- [15] H. D. Willauer, D. R. Hardy, M. K. Lewis, E. C. Ndubizu, F. W. Williams, *Energy Fuels* **2009**, *23*, 1770–1774.
- [16] Jaguar, version 7.6, Schrödinger, LLC, New York, NY, **2009**; www.schrodinger.com.
- [17] a) A. D. Becke, *Phys. Rev. A* **1988**, *38*, 3098–3100; b) J. P. Perdew, in *Electronic Structure Theory of Solids*; (Eds.: P. Ziesche, H. Eschrig), Akademie Verlag, Berlin, **1991**, pp. 11–20; c) J. P. Perdew, J. A. Chevary, S. H. Vosko, K. A. Jackson, M. R. Pedersen, D. J. Singh, C. Fiolhais, *Phys. Rev. B* **1992**, *46*, 6671–6687.
- [18] LACVP basis sets use 6-31G for main group elements and the Hay-Wadt ECP for Fe: P. J. Hay, W. R. Wadt, *J. Chem. Phys.* **1985**, *82*, 299–310.
- [19] a) D. J. Tannor, B. Marten, R. Murphy, R. A. Friesner, D. Sitkoff, A. Nicholls, M. Ringnalda, W. A. Goddard, B. Honig, *J. Am. Chem. Soc.* **1994**, *116*, 11875–11882; b) B. Marten, K. Kim, C. Cortis, R. A. Friesner, R. B. Murphy, M. N. Ringnalda, D. Sitkoff, B. Honig, *J. Phys. Chem.* **1996**, *100*, 11775–11788.
- [20] A. V. Marenich, R. M. Olson, C. P. Kelly, C. J. Cramer, D. G. Truhlar, *J. Chem. Theory Comput.* **2007**, *3*, 2011–2033.
- [21] The LACV3P basis set is a triple-zeta contraction of the LACVP basis set developed and tested at Schrödinger, Inc. LACV3P basis sets use 6–311G for main-group elements.
- [22] K. P. Jensen, J. Cirera, *J. Phys. Chem. A* **2009**, *113*, 10033–10039.
- [23] a) C. Angeli, R. Cimraglia, S. Evangelisti, T. Leininger, J.-P. Malrieu, *J. Chem. Phys.* **2001**, *114*, 10252–10264; b) I. Schapiro, K. Sivalingam, F. Neese, *J. Chem. Theory Comput.* **2013**, *9*, 3567–3580.
- [24] F. Neese, F. Wennmohs, A. Hansen, *J. Chem. Phys.* **2009**, *130*, 114108–114118.
- [25] F. Weigend, R. Ahlrichs, *Phys. Chem. Chem. Phys.* **2005**, *7*, 3297–3305.

Manuscript received: October 17, 2017

Accepted manuscript online: December 15, 2017


Version of record online: ■ ■ ■ ■ 0000

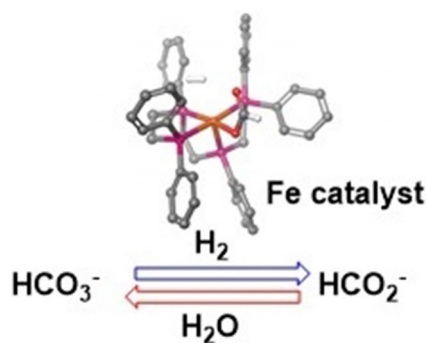
FULL PAPER

Iron Catalysis

R. Marcos, F. Bertini, Z. Rinkevicius,
M. Peruzzini, L. Gonsalvi,
M. S. G. Ahlquist*



 Mechanistic Studies on NaHCO_3
Hydrogenation and HCOOH
Dehydrogenation Reactions Catalysed
by a Fe^{II} Linear Tetrakisphosphine
Complex



The mechanism of Fe -catalysed inter-conversion of bicarbonate and formate was elucidated by theory and supporting experiments.